JGR Planets

RESEARCH ARTICLE
10.1029/2019JE006312

Key Points:
- Evection resonance and a subsequent quasi-resonance regime may remove angular momentum from the Earth-Moon system
- Only a narrow range of fixed tidal parameters can reconcile a high-angular momentum Moon-forming impact with the current Earth-Moon system
- For a time-dependent terrestrial dissipation model, quasi-resonance escape occurs early, leaving the system with an angular momentum excess

Supporting Information:
- Supporting Information S1
- Table S1
- Table S2

Correspondence to:
R. Rufu,
raluca@boulder.swri.edu

Citation:
Rufu, R., & Canup, R. M. (2020). Tidal evolution of the evection resonance/quasi-resonance and the angular momentum of the Earth-Moon system. *Journal of Geophysical Research: Planets*, *125*, e2019JE006312. https://doi.org/10.1029/2019JE006312

Received 3 DEC 2019
Accepted 28 JUL 2020
Accepted article online 13 AUG 2020

Tidal Evolution of the Evection Resonance/Quasi-Resonance and the Angular Momentum of the Earth-Moon System

R. Rufu[1] **and R. M. Canup**[1]

[1]Planetary Science Directorate, Southwest Research Institute, Boulder, CO, USA

Abstract Forming the Moon by a high-angular momentum impact may explain the Earth-Moon isotopic similarities; however, the post-impact angular momentum needs to be reduced by a factor of 2 or more to the current value (1 L_{EM}) after the Moon forms. Capture into the evection resonance, occurring when the lunar perigee precession period equals 1 year, could remove the angular momentum excess. However the appropriate angular momentum removal appears sensitive to the tidal model and chosen tidal parameters. In this work, we use a constant-time delay tidal model to explore the Moon's orbital evolution through evection. We find that exit from formal evection occurs early and that, subsequently, the Moon enters a quasi-resonance regime, in which evection still regulates the lunar eccentricity even though the resonance angle is no longer librating. Although not in resonance proper, during quasi-resonance angular momentum is continuously removed from the Earth-Moon system and transferred to Earth's heliocentric orbit. The final angular momentum, set by the timing of quasi-resonance escape, is a function of the ratio of tidal strength in the Moon and Earth and the absolute rate of tidal dissipation in the Earth. We consider a physically motivated model for tidal dissipation in the Earth as the mantle cools from a molten to a partially molten state. We find that as the mantle solidifies, increased terrestrial dissipation drives the Moon out of quasi-resonance. For post-impact systems that contain >2 L_{EM}, final angular momentum values after quasi-resonance escape remain significantly higher than the current Earth-Moon value.

Plain Language Summary Forming the Moon by a high-angular momentum impact may offer a compelling explanation for measured Earth-Moon isotopic similarities. However, the post-impact system after such an event contains a significantly larger angular momentum than the current Earth-Moon system. As the early Moon tidally recedes, its perigee precession rate decreases. When the precession rate equals 1 year, the Moon may be captured into the evection resonance with the Sun. It was proposed that during this stage the excess angular momentum is removed, but the appropriate angular momentum removal has appeared sensitive to the chosen tidal model. In this work, we find that the Moon exits formal resonance early but may enter a prolonged quasi-resonance regime, in which angular momentum is continuously removed. The final angular momentum, set by the timing of the quasi-resonance escape, is a function of the relative tidal strength in the Moon and Earth and the absolute tidal dissipation in the planet. We explore the tidal evolution through evection resonance during planetary cooling adopting a recent model for Earth's time-dependent tidal dissipation and find that the Moon is driven out of quasi-resonance before sufficient angular momentum is removed, inconsistent with the Earth-Moon value.

1. Introduction

The leading theory of lunar origin posits that a Mars-sized protoplanet impacted the proto-Earth at the late stages of its accretion (Cameron & Ward, 1976). An oblique impact with an angular momentum (AM) close to that in the current Earth-Moon system ($L_{EM} = 3.5 \cdot 10^{41}\,g\,cm^{-2}\,s^{-1}$) generates a debris disk up to two times more massive than the Moon (Canup & Asphaug, 2001; Canup, 2004), which later may accrete to form a lunar-sized satellite (Ida et al., 1997; Salmon & Canup, 2012). Such a "canonical" giant impact is able to account for the AM in the current Earth-Moon system and the Moon's depletion in iron and volatile elements (Canup et al., 2015). However, the disk created by a canonical impact is mainly derived from the impactor, while the Earth largely retains its pre-impact composition, which would nominally produce a Moon that is compositionally distinct from Earth's mantle. This is in contrast to high-precision measurements of lunar isotopes, which indicate that the Moon and Earth have essentially identical isotopic compositions in most elements (e.g., in oxygen, Herwartz et al., 2014; titanium, Zhang et al., 2012).

Instead, certain types of high-AM impacts can create a debris disk and a planet that have nearly equal proportions of impactor material, offering a compelling mechanism to create a satellite that is compositionally similar to the silicate Earth (Ćuk & Stewart, 2012; Canup, 2012, see also Lock et al., 2018). However, the post-impact Earth-Moon AM is typically $\gtrsim 2\,L_{\rm EM}$ and must be greatly reduced after the Moon forms for such models to be viable.

A promising mechanism to reduce the Earth-Moon system AM to its current value involves a solar resonance called evection (Brouwer & Clemence, 1961; Ćuk & Stewart, 2012; Kaula & Yoder, 1976; Touma & Wisdom, 1998), which occurs when the period of precession of the lunar perigee equals 1 year. During evection, the angle between the Sun and Moon at lunar perigee (or apogee) maintains a nearly constant value $\sim\pi/2$. As the Moon's orbit expands due to tidal interaction with the Earth, the net solar torque increases the lunar eccentricity, and AM is transferred from the Earth-Moon pair to Earth's orbit around the Sun. For an initial 5-hr terrestrial day (corresponding to Earth's spin after a canonical giant impact, Canup, 2004), evection is encountered at 4.6 Earth radii ($R_\oplus$), and only limited AM removal was found (Touma & Wisdom, 1998). However for a high-AM giant impact (total AM $\gtrsim 2L_{\rm EM}$), the resonance location shifts outward due to Earth's increased spin and oblateness, and large-scale AM removal was found (Ćuk & Stewart, 2012). Notably, for these cases there also appeared to be a preference for a final AM near $\sim 1\,L_{\rm EM}$, independent of the starting AM (Ćuk & Stewart, 2012).

Ćuk and Stewart (2012) used a simplified approximation of a constant lag angle (constant-Q) tidal model. Later studies with a full constant-Q model found that the formal evection resonance is unsuccessful at appropriately reducing the Earth-Moon AM (Tian et al., 2017; Wisdom & Tian, 2015). For cases with a large terrestrial tidal dissipation factor, Q, it was found that capture into proper evection resonance did not occur but that instead the Moon was captured into a limit cycle associated with evection, in which appropriate AM can be lost even though the evection resonance angle is not librating (Tian et al., 2017; Wisdom & Tian, 2015).

Motivated by these differences, we seek to understand whether evection can remove sufficient AM, as this is key for assessing the overall likelihood of high-AM lunar origin scenarios. Recent evection studies (Ćuk & Stewart, 2012; Tian et al., 2017; Wisdom & Tian, 2015) have used N-body codes. In this work we use a complementary semi-analytical model (Ward et al., 2020, see also Ward & Canup, 2013) and test a broader range of tidal parameters, which would be computationally prohibitive with N-body methods.

In Ward et al. (2020), we developed a simplified model for evection, in which the libration of the resonance angle about $\sim\pi/2$ was assumed to be small. That study estimated that shortly after capture, the Moon's eccentricity becomes large enough to cause its orbit to contract, the libration amplitude increases, and escape from resonance occurs before much AM is removed from the system. However, the approach in Ward et al. (2020) could not treat nonlibrating behavior. In this study, we track the libration of the resonance angle during the encounter with evection resonance, assess the timing of resonance escape and the subsequent evolution, and estimate the final AM of the system as a function of tidal parameters. We consider both time-constant tidal parameters and cases in which the terrestrial tidal dissipation factor varies with time as the Earth's mantle cools and begins to solidify (Zahnle et al., 2015).

2. Model

We here briefly describe our tidal and evection model (see Ward et al., 2020, for more details). We assume the Moon forms on a low-eccentricity (e) orbit, at a semimajor axis (a) slightly beyond the Roche limit, consistent with the lunar orbit after accretion (Ida et al., 1997; Salmon & Canup, 2012, 2014). The formation of the Moon from a debris disk implies an initially low-inclination, near-equatorial orbit (Ida et al., 1997), which is inconsistent with the $\sim 5°$ inclination of the current Moon's orbit relative to the ecliptic (Ćuk et al., 2016; Goldreich, 1966; Touma & Wisdom, 1994). Later collisionless encounters of the Moon with the leftover planetesimal population could potentially excite the lunar inclination when it is more distant (Pahlevan & Morbidelli, 2015). As evection occurs early and close to the planet, we assume that the lunar inclination relative to the planetary equatorial plane is small throughout the modeled encounter with evection.

We consider the coplanar problem in which the orbital and equatorial planes of the Earth and Moon are aligned. The scalar AM of the Earth-Moon is

$$L \sim Cs + C_m s_m + m\sqrt{GM_{\oplus} a(1-e^2)} \quad (1)$$

where G is the gravitational constant, $M_{\oplus} = 5.97 \cdot 10^{27}$ g [$m = 7.34 \cdot 10^{25}$ g], C [C_m], and s [s_m] are Earth's [Moon's] mass, moment of inertia, and spin rate, respectively (here we assume that $(1 + m/M_{\oplus})^{-1/2} = 0.994 \sim 1$). We normalize the AM by $C\Omega_{\oplus}$, where $\Omega_{\oplus} = \sqrt{GM_{\oplus}/R_{\oplus}^3}$ is the orbital frequency at 1 Earth radius ($R_{\oplus}$), giving

$$L' = s' + \kappa s'_m + \gamma\sqrt{a'(1-e^2)} \quad (2)$$

where primes indicate normalized values ($s' = s/\Omega_{\oplus}$, $s'_m = s_m/\Omega_{\oplus}$, and $a' = a/R_{\oplus}$), $\kappa \equiv C_m/C = 1.07 \cdot 10^{-3}$ is the ratio of the maximum principal moments of inertia of the two bodies, $\gamma \equiv \mu/\lambda = 0.0367$, with μ being the Moon-to-Earth mass ratio and $\lambda \equiv C/M_{\oplus} R_{\oplus}^2 = 0.335$ the Earth's gyration constant. Specifically, L' is the ratio of the total AM to that of a single object having Earth's mass and moment of inertia, rotating at $\Omega_{\oplus}$, which is close to the critical rotation rate before break-up. In these units, the current Earth-Moon AM is $L'_{\mathrm{EM}} \approx 0.35$.

Tidal interactions between the Earth and Moon exchange AM between the objects' spins and the lunar orbit, while maintaining the total AM constant. Tides raised on the Earth by the Moon (Earth tides) alter s', while tides raised on the Moon by Earth (lunar tides) alter s'_m (we nominally assume a non-synchronous lunar rotation; see section 3.3 for cases assuming synchronous lunar rotation). The tidal changes to Earth's (s') and Moon's (s'_m) spin are

$$\dot{s}' = -\frac{1}{2}\gamma\sqrt{a'(1-e^2)}\left(\frac{\dot{a}'_{\oplus}}{a'} - \frac{2e\dot{e}_{\oplus}}{1-e^2}\right) \quad (3)$$

$$\dot{s}'_m = -\frac{1}{2}\frac{\gamma}{\kappa}\sqrt{a'(1-e^2)}\left(\frac{\dot{a}'_m}{a'} - \frac{2e\dot{e}_m}{1-e^2}\right) \quad (4)$$

with the $\dot{a}'_{\oplus}$ and $\dot{e}'_{\oplus}$ [$\dot{a}'_m$ and $\dot{e}'_m$] representing rates of change due to Earth [lunar] tides.

The time derivatives in Equations 3 and 4 (and henceforth) use a normalized time variable $\tau = t/t_T$, where t_T is a tidal time constant and, defined by $t_T \equiv (6k_{2\oplus}\mu\Omega_{\oplus}^2\Delta t)^{-1}$, where Δt is the terrestrial tidal time delay (see below), and $k_{2\oplus}$ is Earth's Love number, where we set $k_{2\oplus} \sim 0.3$ (Murray & Dermott, 1999). For example, the current terrestrial tidal factor $Q \sim 12$ (Murray & Dermott, 1999) corresponds to a time lag of $\Delta t \sim 10$ min and $t_T \sim 13.6$ hr for the current s and n of the Earth-Moon (where n is the lunar mean motion).

All common tidal models used for long-term integrations make simplifying assumptions. We employ the tidal model developed by Mignard (1979, 1980), which makes two main assumptions. First, that the tidal distortion due to the perturbing body can be accurately described as an additional second-order term ($l = 2$) in the potential of the perturbed body. Second, that in each body, the formation of the equilibrium tide is delayed by some time, Δt, relative to the tide-raising perturbation, and that this time delay does not depend on the frequency of the tidal response. The time delay reflects the effects of dissipation in the distorted body, which can be different for each body (i.e., Δt for the Earth can be different than Δt_m for the Moon). A key advantage of the Mignard model is its physically intuitive treatment for eccentric orbits and those near the corotation distance (where the Moon's orbital period equals the Earth's day), both conditions that can apply to evolution in evection (see supporting information Text S1 for more details). In the Mignard model, the orbit-averaged tidal lag angle, δ, between the equilibrium Earth tide and the sublunar position is given by $\delta = (s - n)\Delta t$. The lag angle is then frequency-dependent, and the resulting torque smoothly approaches zero for a circular orbit as corotation is approached and $n \to s$. In contrast, a constant-Q model (e.g., Kaula, 1964) assumes the tidal response is delayed by a fixed phase, rather than by a fixed time, relative to the tide-raising potential. A difficulty is that the resulting lag angle varies discontinuously as the frequency associated with each term passes through zero; for example, for the semidiurnal tide on the Earth, the lag angle abruptly changes from a positive (leading) to a negative (trailing) value for orbits just outside to just inside the

corotation radius, and there is no variation in the size of the lag angle based on the closeness of the orbit to corotation (e.g., Ćuk et al., 2016).

The known responses of the current Earth and Moon can be compared to predictions of tidal models. For a tidal dissipation factor, Q, that varies with frequency χ as $Q \propto \chi^{\tilde{\alpha}}$, the Mignard model predicts $\tilde{\alpha} = -1$, while the constant-Q model predicts $\tilde{\alpha} = 0$. Seismic measurements imply $\tilde{\alpha} = 0.2$ to 0.4 for the current terrestrial mantle (e.g., Efroimsky & Lainey, 2007), while analyses of lunar laser ranging (LLR) data suggest $\tilde{\alpha}$ values that are small but negative for the current Moon (Williams et al., 2014; Williams & Boggs, 2015). Thus LLR data seem better described by a constant-Q model, although tidal models in which dissipation peaks at a certain frequency (plausibly simulating the effect of a low-viscosity layer) seem to most successfully fit the current lunar measurements (Williams & Boggs, 2015). However, the extent to which these results bear on the initial Earth and Moon is unknown, particularly for the postgiant impact Earth that was likely molten and fluid-like in its tidal response (see below). We adopt the Mignard model as a reasonable proxy for the initial Earth-Moon system. The Mignard lag time can be related to a tidal quality factor, Q, as $Q \sim (\psi \Delta t)^{-1}$, where ψ is the frequency of oscillation. For the Earth, the semidiurnal lunar tide frequency is $2|s - n|$, where the factor of 2 arises because there are two tidal cycles for each synodic period (e.g., Efroimsky & Lainey, 2007; Peale & Canup, 2015). For ease of comparison with previous works, we express results as a function of an effective terrestrial tidal dissipation factor, $Q_{\rm eff}$, where $Q_{\rm eff} = (2(s_0 - n_0)\Delta t)^{-1}$, and s_0 and n_0 are the initial values of s and n in our simulations. However, our actual simulations utilize Δt and A as defined in Equation 9below, rather than $Q_{\rm eff}$.

Mignard,'s (1980) normalized equations for the rates of change of a' and e due to Earth's tidal dissipation (Earth tides) read (e.g., Ward et al., 2020)

$$\frac{\dot{a}'_{\oplus}}{a'} = (\mu + 1)\left(\frac{s' a'^3/2 f_1(e) - f_2(e)}{a'^8}\right) \tag{5}$$

$$\dot{e}_{\oplus} = e(\mu + 1)\left(\frac{s' a'^3/2 g_1(e) - g_2(e)}{2a'^8}\right) \tag{6}$$

where f_1, f_2, g_1, and g_2 are functions of e found by averaging the tidal forces over one lunar orbit (see Table S1 Mignard, 1980; Meyer et al., 2010; Ward et al., 2020).

For nonsynchronous lunar rotation, the corresponding rates due to lunar tidal dissipation (lunar tides) are

$$\frac{\dot{a}'_m}{a'} = A(\mu + 1)\left(\frac{s'_m a'^{3/2} f_1(e) - f_2(e)}{a'^8}\right) \tag{7}$$

$$\dot{e}_m = eA(\mu + 1)\left(\frac{s'_m a'^{3/2} g_1(e) - g_2(e)}{2a'^8}\right) \tag{8}$$

where A is the relative strength of lunar tides compared to Earth tides, defined as

$$A \equiv \frac{k_{2m}}{k_{2\oplus}} \frac{\Delta t_m}{\Delta t} \left(\frac{M_{\oplus}}{m}\right)^2 \left(\frac{R_m}{R_{\oplus}}\right)^5 \tag{9}$$

where $k_{2\oplus}$ [k_{2m}], Δt [Δt_m], and $R_{\oplus}$ [R_m] are Earth's [Moon's] Love number, tidal lag time, and radius, respectively. When $A \gg 1$, tidal dissipation in the Moon is stronger than in the planet, and hence in this case, lunar tides (which typically decrease a and e) are stronger than Earth tides (which typically increase a and e). Shortly after the giant impact, A was likely $\gg 1$, because Earth was fully molten and surrounded by a thick atmosphere (leading to a fluid-like response with a small Δt), whereas the Moon would have cooled more quickly to a dissipative partially solid state (with a larger Δt_m) by the time the Moon encountered the evection resonance (Zahnle et al., 2015, see section 3.4).

The Moon initially evolves outward due to tides until it reaches the semimajor axis at which resonance occurs ($a'_{\rm res}$). The effect of evection on the lunar eccentricity is (Brouwer & Clemence, 1961; Ward et al., 2020)

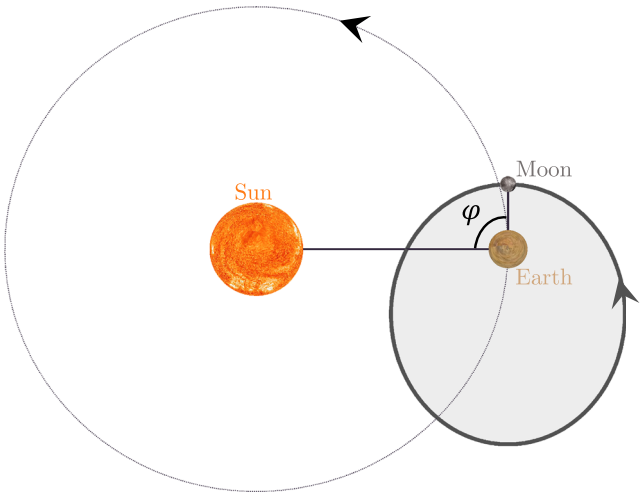

Figure 1. Schematic of the Earth's (dashed line) and lunar (solid line) orbit. During proper evection, the angle between the Sun and the Moon at perigee (with Earth as the reference point) librates about $\varphi \sim \pm\pi/2$, with perigee occurring either on the leading side compared to Earth's heliocentric motion (as seen here) or on the trailing side. Distances and sizes are not to scale.

$$\frac{de_{\rm res}}{d\tau} = \dot{e}_{\rm res} = \frac{15}{4} e\sqrt{(1-e^2)}a'^{3/2}(\Omega_\odot t_T)\frac{\Omega_\odot}{\Omega_\oplus}\sin(2\varphi) \tag{10}$$

where $\varphi = \varpi - \lambda_\odot$ is the angle between the Moon's longitude of perigee, ϖ, and the solar longitude, $\lambda_\odot$, with Earth as the reference point (Figure 1), and $\Omega_\odot = \dot{\lambda}_\odot$ is Earth's orbital frequency.

The phase angle, φ, is altered by solar interactions and Earth's quadrupole gravitational field (Ward et al., 2020):

$$\frac{d\varphi}{d\tau} = \dot{\varphi} = \left[\frac{\Lambda^2 s'^2}{a'^{7/2}(1-e^2)^2} - 1 + \frac{3}{4}\sqrt{1-e^2}a'^{3/2}\left(\frac{\Omega_\odot}{\Omega_\oplus}\right)(1+5\cos 2\varphi)\right]\Omega_\odot t_T \tag{11}$$

where we assume that Earth's oblateness is a function of its spin, $J_2 = J_\star s'^2$ ($J_\star = 0.315$), and define $\Lambda \equiv \sqrt{3/2 J_\star \Omega_\oplus/\Omega_\odot} = 54.2$. In the vicinity of evection, when $a'_{\rm res} = \left[\Lambda s'/(1-e^2)\right]^{4/7}$, the apsidal precession rate, $\dot{\varpi}$, approaches Earth's orbital frequency, $\Omega_\odot$, and the first term on the right-hand side in Equation 11 is ~1. In that case, the resonance angle librates slowly because the term proportional to $\Omega_\odot/\Omega_\oplus$ is $\ll$1.

For given values of s' and a', one can find the stationary points at which $\dot{e}_{\rm res}$ and $\dot{\varphi}$ vanish. From Equation 10 we must have $\varphi \approx 0, \pm\pi/2, \pi$, and from Equation 11the stable stationary (e_s) and unstable saddle (e_{sx}) eccentricity points solve the equations

$$\frac{\Lambda^2 s'^2}{a'^{7/2}(1-e_s^2)^2} - 1 - 3\sqrt{1-e_s^2}a'^{3/2}\frac{\Omega_\odot}{\Omega_\oplus} = 0 \tag{12}$$

$$\frac{\Lambda^2 s'^2}{a'^{7/2}(1-e_{sx}^2)^2} - 1 + \frac{9}{2}\sqrt{1-e_{sx}^2}a'^{3/2}\frac{\Omega_\odot}{\Omega_\oplus} = 0 \tag{13}$$

Finally $e = 0$ is also a stationary point for which $\dot{e}_{\rm res} = 0$ and φ is undefined. In the absence of tidal dissipation, the solar terms do not alter the overall energy of the system; hence an integral of motion defines the allowed values of (e,φ). Level curve diagrams for different energies are shown in Figure 2.

Initially after the Moon encounters evection, e_s is small and e_{sx} is not defined (i.e., Equation 13 has only imaginary solutions), corresponding to what we will call shallow resonance (Figure 2a). As Earth's spin, s', decreases and/or a' increases, e_s increases as well (moves up the y-axis) and an unstable point appears at the origin ($e_{sx} = 0$; Figure 2b). In shallow resonance, there are two regimes: for low energy levels (blue colors in Figure 2b), trajectories librate around a stable point ($e_s, \pm\pi/2$), while higher energies (red colors in Figure 2b) circulate around both stable points. Further in the evolution, in what we refer to as deep resonance, at a certain energy level the trajectory intersects the saddle points (e_{sx}, 0),(e_{sx}, π), dividing the phase space into three regions (separatrix curve; dashed line in Figure 2c). As continued evolution drives the level curves outward, the inner region around the origin occupies a larger part of the phase space (Figure 2d). In this inner region, trajectories circulate about the origin in a clockwise motion, while beyond the outer separatrix, trajectories circulate both stationary points in a counter-clockwise motion. The intermediate, increasingly crescent-like region is that of resonant libration, in which trajectories travel in an overall counter-clockwise sense.

As seen from the snapshots in Figure 2, the trajectories are symmetric around the y-axis; therefore, in the absence of tidal evolution, evection alone does not alter the AM of the system because there is no net solar torque ($T \propto e^2 \sin 2$ Ward et al., 2020). However, the gradual evolution of the level curves, due to tidal dissipation, disrupts the y-axis symmetry (i.e., the actual trajectories are no longer closed), and AM is removed

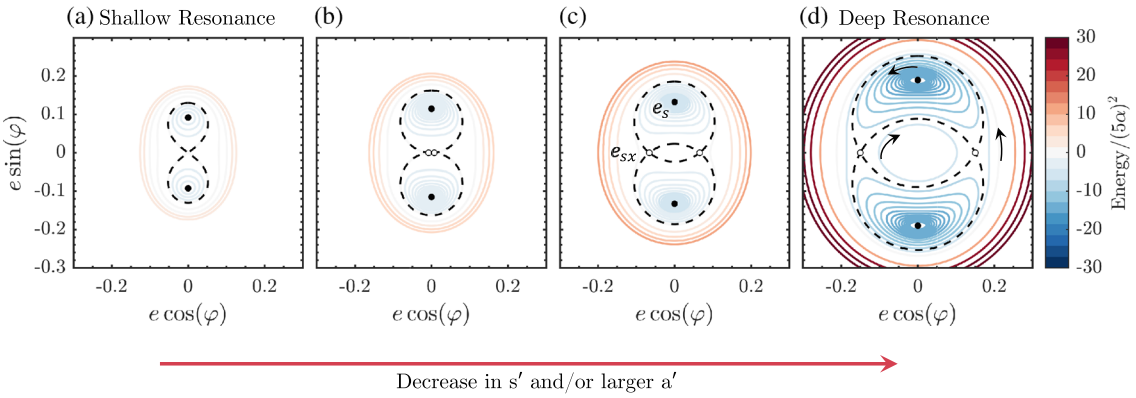

Figure 2. Example level curves for different energies (depicted as different colors). The Sun is in the direction of the positive *x*-axis. The small full [empty] circles represent the stable [unstable] stationary points, e_s [e_{sx}]. The dashed curves are the separatrix that divides the phase space into as many as three regions: libration around one stable stationary point (evection proper), circulation around the origin, and circulation around all stationary points. The panels show different evolution stages: (a) shallow resonance, when the unstable stationary point is not defined (Equation 13 has no real solution); (b) as the planetary spin, s', decreases and/or the lunar semimajor axis, a' increases, the resonance further develops (e_s and e_{sx} increase). (c) Deep resonance, defined as the stage when $e_{sx} > 0$ and the central circulating region between the unstable saddle points emerges. (d) Further evolution causes the central area between the saddle points to occupy an increasing portion of the phase diagram. Arrows in panel (d) show the direction of trajectory motion. The energy levels are normalized by $(5\alpha)^2$, where $\alpha \equiv 3/8a'^{3/2}\Omega_\odot/\Omega_\oplus$.

from the system. While *not* in evection resonance, Earth and lunar tides alter the semimajor axis and eccentricity (Equations 5–8), which is directly balanced by the changes in Earth's and lunar spins (Equations 3 and 4), so that the total AM of the system (Equation 1) remains constant. During evection resonance, tides still control the semimajor axis and spin evolutions, but so long as the rate of change of the eccentricity is controlled by evection (Equation 10), the total AM is no longer constant. Instead, AM from the Earth-Moon system is transferred to Earth's orbit around the Sun.

To model the Earth-Moon system as it tidally evolves and encounters evection, we integrate the equations for the Earth and lunar spin rates (Equations 3 and 4), the Moon's semimajor axis ($\dot{a} = \dot{a}_\oplus + \dot{a}_m$, using Equations 5 and 7), eccentricity ($\dot{e} = \dot{e}_\oplus + \dot{e}_m + \dot{e}_{\rm res}$, using Equations 6, 8, and 10) and the resonance angle (Equation 11). We use the "VODE" (Variable-coefficient Ordinary Differential Equation, Brown et al., 1989) integrator in *SciPy* package (Virtanen et al., 2019). We assume a minimum eccentricity of $e = 10^{-8}$, which approximates the minimum eccentricity expected due to excitation from collisionless encounters when the Moon's semimajor axis is small (e.g., Pahlevan & Morbidelli, 2015; Spurzem et al., 2009). The derivative at the minimum eccentricity is set to $\dot{e} = \dot{e}_{res}$, limiting further eccentricity decrease due to tides but allowing the solar terms to increase the eccentricity when evection occurs (see Text S2). We stop the integration if the Moon's perigee is $<2\ R_\oplus$ (a tidal disruption boundary for high-*e* orbits, Sridhar & Tremaine, 1992) or if the lunar spin rate, the Earth's spin rate, and the Moon's mean motion are equal (i.e., if the system reaches the double synchronous state).

3. Results

At the start of each simulation, $e = 0.01$ (e.g., Salmon & Canup, 2012) and $a' = 3.5$. We assume an initial terrestrial spin of 2 hr, which corresponds to a total AM of $L' = 0.77$ (i.e., $L = 2.2\ L_{\rm EM}$, consistent with high-AM Moon forming impacts, Ćuk & Stewart, 2012; Canup, 2012). The tidal time constant, t_T (which is proportional to $\Delta t^{-1} \propto Q_{\rm eff}$), the relative tidal strength, A, and $0 \le \varphi(0) \le 2\pi$ are input parameters.

The remainder of section 3 is organized as follows. First, we describe in section 3.1 the evolution assuming that the Moon's rotation evolves solely due to tides (implying nonsynchronous lunar spin for eccentric orbits) and for relatively low A and Δt values that are constant in time, similar to conditions considered in Ćuk and Stewart (2012) (their Figure 4b; purple line). Next, we compare the final AM after encounter with evection across a large range of tidal parameters, again assuming that A and Δt are constant in time throughout the evolution (for nonsynchronous lunar rotation in section 3.2, and for synchronous lunar rotation in section 3.3). In section 3.4, we consider the most physically plausible initial condition with large A and

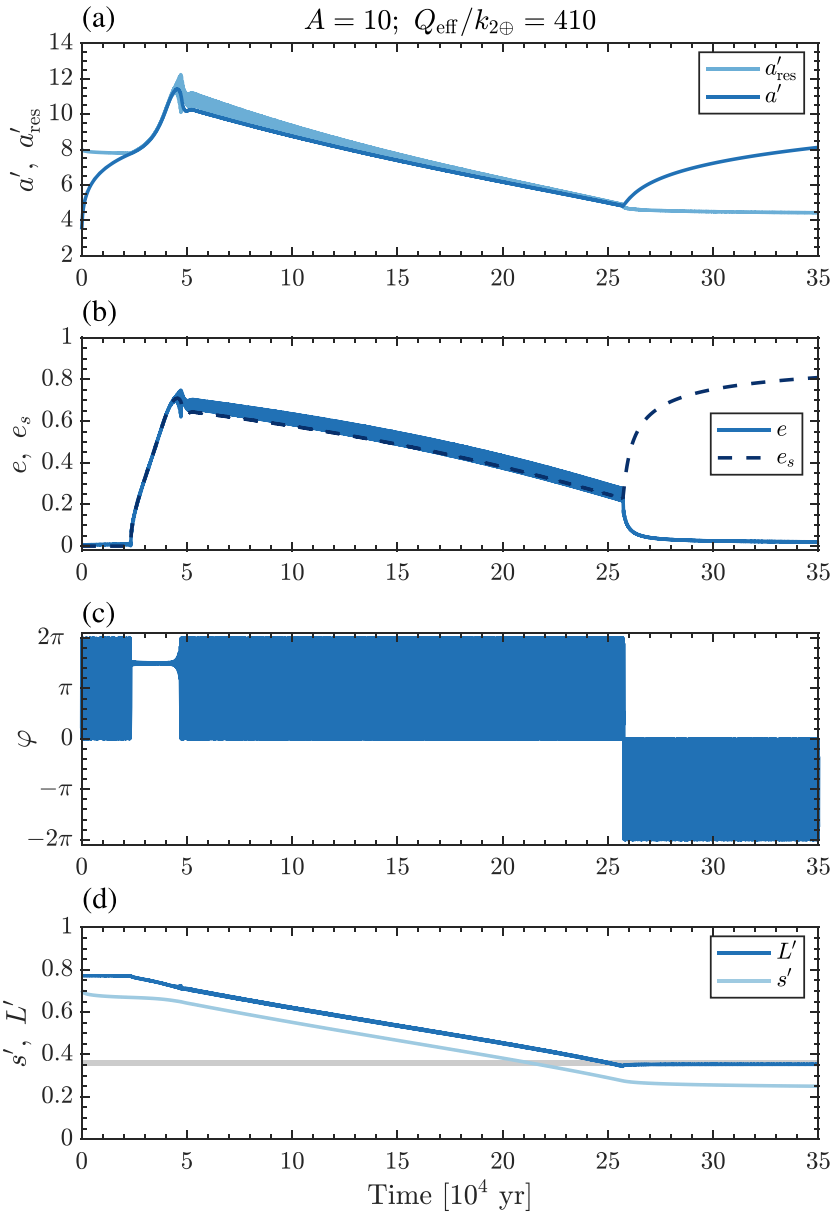

Figure 3. Tidal evolution of the Earth-Moon system for $A = 10$ and terrestrial tidal parameters $Q_{\rm eff}/k_{2\oplus} = 410$ ($t_T = 4.9 \times 10^6$ s). We assume that the Moon's rotation evolves solely due to tides (i.e., nonsynchronous lunar spin for eccentric orbits). (a) Normalized lunar semimajor axis (dark blue) and position of evection resonance (light blue) semimajor axis; (b) eccentricity (solid line) and stable stationary eccentricity (dashed line- numerically calculated by solving Equation 12); (c) resonance angle (d) normalized AM (dark blue) and terrestrial spin (light blue) as a function of time (see text for details). For the initial AM of $L' = 0.77$ ($L \sim 2.2\ L_{\rm EM}$), evection resonance is encountered at $a = 7.8\ R_\oplus$. The horizontal gray area represents values consistent with the current Earth-Moon, accounting for later AM change due to solar tides and late accretion impacts (Bottke et al., 2010; Canup, 2004). We set negative values for the resonance angle, φ, when the derivative $\dot{\varphi}$ is negative, indicating that the lunar precession period is >1 year and that the trajectory moves in the clockwise direction on the phase diagram in the central circulation region. For comparison today's values are $A \sim 13$ and $Q_{\rm eff}/k_{2\oplus} \sim 40$ (Murray & Dermott, 1999; Williams & Boggs, 2015).

large $Q_{\rm eff}/k_{2\oplus}$, and we adopt a time-dependent terrestrial dissipation model to describe the Moon's evolution through evection resonance during Earth's gradual solidification after a giant impact (Zahnle et al., 2015).

3.1. Resonance and Quasi-Resonance Evolution

Figure 3 shows the results from an integration with $A = 10$ and $Q_{\rm eff}/k_{2\oplus} \approx 410$. Initially, the Moon's orbit expands at a low eccentricity due to Earth tides, until it is captured in the evection resonance at $a' = 7.77$

(Figure 3a). The resonance drives an increase in eccentricity (solid line in Figure 3b) as the orbit further expands due to Earth tides ($|\dot{a}_{\oplus}| > |\dot{a}_m|$). During this outbound phase, e closely follows the stable stationary eccentricity, e_s (dashed line in Figure 3b), and the resonance angle librates about $\varphi \sim \pi/2$ with small amplitude (Figure 3c). The trajectory is librating within the phase diagram region surrounding the stable stationary point with a counter-clockwise motion (Figure 2). Only modest AM ($\lesssim$10%) is removed during this phase.

As the eccentricity grows further, lunar tides become stronger, eventually overcoming the orbital expansion driven by Earth tides and causing the semimajor axis growth to stall when $a' \approx 11.4$ and $e \approx 0.7$. From this point, the orbit contracts ($|\dot{a}_{\oplus}| < |\dot{a}_m|$), the libration amplitude increases until it reaches the saddle point (e_{sx}, 0), and the trajectory exits the resonant region. In this simulation, escape occurs to the high-e side into the region beyond the outer separatrix (Figure 2), where the resonance angle no longer librates but instead circulates across all values between 0 and 2π (Figure 3c) in a counter-clockwise sense on the phase diagram. The Moon is now not in evection proper, but it enters a prolonged phase in which evection still regulates the secular evolution of the Moon's eccentricity. We call this state quasi-resonance (QR).

In QR, the Moon's precession period is somewhat less than 1 year, and the Moon's orbit is interior to the position of the resonance. The Moon's orbit continues to contract inward due to the predominance of lunar tides. However, as the lunar semimajor axis decreases, the position of evection resonance ($a_{\rm res}$, light blue Figure 3a) moves inward at a somewhat faster rate because of the ongoing decrease in Earth's spin, s', and the associated reduction in Earth's J_2. Hence with time the resonance converges on the Moon's orbit from the outside. During QR, tides drive the trajectory downward on the phase diagram (Figure 2), but they are blocked by evection when it approaches the separatrix from above, which forces the trajectory to maintain a minimum eccentricity of $\approx e_{sx}$. So long as the tidal change is slow compared to the circulation period, the evolution is adiabatic, and the system continues to circulate just above the separatrix. Even though φ is circulating, because evection continues to maintain $e \gtrsim e_{sx}$, AM is transferred from the Earth-Moon system to Earth's orbit. It is during this QR regime that substantial AM is removed (Figure 3c).

In QR, the trajectory closely hugs the outer separatrix as φ circulates from 0 to 2π, with the eccentricity oscillating between a minimum value $e_{\rm min} \sim e_{sx}$ when near the x-axis on the phase diagram, and a maximum value $e_{\rm max} \sim e_+$ comparable to that of the outer separatrix curve near the y-axis on the phase diagram (see Figure S3). To the order e^4 and for deep resonance, the later can be expressed as $e_+^2 = e_s^2 + \sqrt{5\alpha e_*^2}$, where $e_*^2 \equiv (e_s^2 + e_{sx}^2)/2 \sim 1 - \alpha - \Lambda s'/a'^{7/4}$, and $\alpha = 3/8 a'^{3/2} \Omega_\odot/\Omega_\oplus$ (Ward et al., 2020). For shallow resonance, the unstable stationary eccentricity is not defined and $e_+^2 = 2e_s^2$ (Ward et al., 2020). At the level of an order e^4 approximation, Equation 11 can be expressed as $\dot{\varphi} = 2\Omega_\odot t_T \left(e^2 - e_*^2 + 5\alpha \cos 2\varphi\right)$ (Ward et al., 2020), implying an angle-averaged circulation rate $\langle\dot{\varphi}\rangle = 2\Omega_\odot t_T \left(\langle e^2\rangle - e_*^2\right)$, where for deep resonance, $\langle e^2\rangle \sim (e_{\rm min}^2 + e_{\rm max}^2)/2 \sim e_*^2 + \sqrt{5\alpha e_*^2}$ (or for shallow resonance, $\langle e^2\rangle \sim e_*^2 + 5\alpha$). The time to complete an eccentricity oscillation cycle is

$$P_{\rm circ;deep} = \pi/\dot{\varphi} = \frac{\pi}{2 t_T \Omega_\odot \sqrt{5\alpha} e_*}; \; P_{\rm circ;shallow} = \frac{\pi}{2 t_T \Omega_\odot 5\alpha} \tag{14}$$

where $P_{\rm circ;deep}$ [$P_{\rm circ;shallow}$] refers to the period of oscillations during deep resonance [shallow resonance].

The timescale for tides to cause the eccentricity to decrease to a value less than e_{sx} is approximately

$$t_{\rm cross} = (e - e_{sx})/|\dot{e}_{\oplus} + \dot{e}_m| \tag{15}$$

While the circulation timescale (Equation 14; dark blue line Figure 4b) increases as e and a' decrease, the tidal crossing timescale (Equation 15; light blue line Figure 4b) generally decreases as the eccentricity gradually approaches e_{sx}. When these timescales become comparable, tides drive the Moon inward across the separatrix into the inner nonresonant region when $\varphi \approx 0$ or π (i.e., when the trajectory is near the x-axis on the phase diagram). This is the end of the QR regime.

Beyond this point, the Moon's eccentricity rapidly decreases due to lunar tides, and its semimajor axis accordingly restarts its expansion. The evection resonance is now interior to the Moon, and its position continues to move inward as Earth's spin decreases. Therefore the relative positions of the Moon and the resonance diverge with time, and evection no longer affects the lunar orbit. Further evolution occurs at a nearly

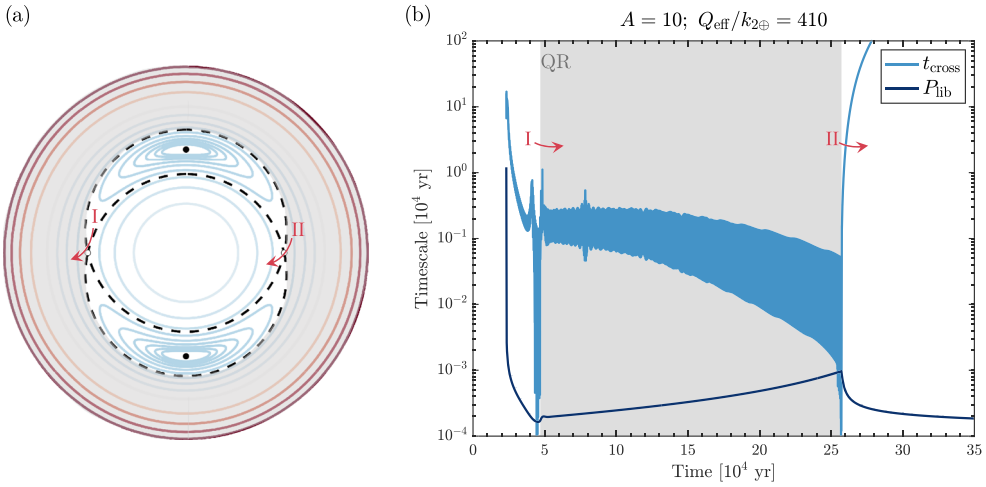

Figure 4. Evolution from resonance to quasi-resonance. (a) Schematic of the level curves (similar to Figure 2 with the QR region highlighted by the gray area. Arrow I [II] depicts the path taken to exit evection proper [QR regime]. (b) The timescale required for tides to drive the eccentricity across the separatrix ($t_{\rm cross}$, light blue; calculated using Equation 15 and averaging over a 100 year period) compared to the timescale of circulation ($P_{\rm circ}$; dark blue) for the evolution depicted in Figure 3 ($A = 10$ and $Q_{\rm eff}/k_{2\oplus} = 410$). The gray area represents the time the system is in the QR regime. When the two timescales are comparable, the trajectory is pushed across the separatrix. At $\sim 4 \cdot 10^4$ year the libration amplitude increased, and the system is pushed from the librating resonant area across the separatrix, exiting proper evection and entering the QR-regime (arrow I). At $\sim 25 \cdot 10^4$ year tides drive the system across the separatix into the central region where clockwise circulation occurs around the origin (arrow II). Once this occurs, the QR-regime ends.

constant Earth-Moon AM via standard tidal evolution. In the simulation shown in Figure 3, the final AM is close to current AM of the Earth-Moon system (gray area in Figure 3d). As described in section 3.2, the final AM depends on when escape from QR occurs, which depends on tidal parameters.

Whenever escape from proper evection resonance places the trajectory in the outer circulating region (i.e., to the high-e side of evection resonance), a QR-regime follows. This occurs in 100% of cases in which $A \gtrsim$ few hundred, because for these cases the resonance is in the shallow resonant regime (Figures 2a–2b) at the time of escape and only the outer circulating region exists. For lower A, the deep resonance regime (Figures 2c–2d) applies at the time of escape, and it is possible for the Moon to also escape from evection proper to the low eccentricity side of the librating region (i.e., into the central circulating region on the phase diagram; see Figure S4 for an example of this evolution). In this case, the lunar orbit is exterior to the position of evection, $a'_{\rm res}$, upon escape, and no QR regime occurs, leaving the Earth-Moon AM at a very high value. Two cases out of 10 simulation performed for the combination of A and t_T in Figures 3 and S4, but with different initial resonance angles, $\varphi(0)$, experienced this non-QR behavior. The probability of exiting the resonance above/below the stable eccentricity varies according to the tidal parameters, as these affect the shape and relative area of the non-QR circulating region (Figures 2c–2d). In general, as the relative tidal strength A decreases, the maximum critical eccentricity before orbit contraction increases (see next section), and escape may increasingly occur into the non-QR region (i.e., the central circulating region). However we find that even for $A \sim$unity, escape usually occurs into the QR region.

3.2. Dependence on Tidal Parameters

Evection resonance and the subsequent QR can remove adequate AM to be consistent with the current Earth-Moon (gray area in Figure 3). In order to estimate the likelihood of such potentially successful cases (final AM $\sim L_{\rm EM}$), we performed simulations across a large range of tidal parameters, $5 \le A \le 10^4$ and $20 \le Q_{\rm eff}/k_{2\oplus} \le 10^5$.

Initial capture into evection resonance requires that the time for the upward movement of the stationary point, $e_s/|\dot{e}_s|$, is longer than the period of libration around that point ($P_{\rm lib} = \pi/4\Omega_\odot t_T \sqrt{5\alpha e_*^2}$, Ward et al., 2020). Therefore, there is a minimum eccentricity for capture $e_{\rm crit} \propto \sqrt{1/t_T}$. For large A values, the eccentricity derivative during the tidal evolution toward evection resonance is negative ($|\dot{e}_\oplus| < |\dot{e}_m|$). Eventually, for strong enough lunar tides the eccentricity at the evection resonance position is smaller

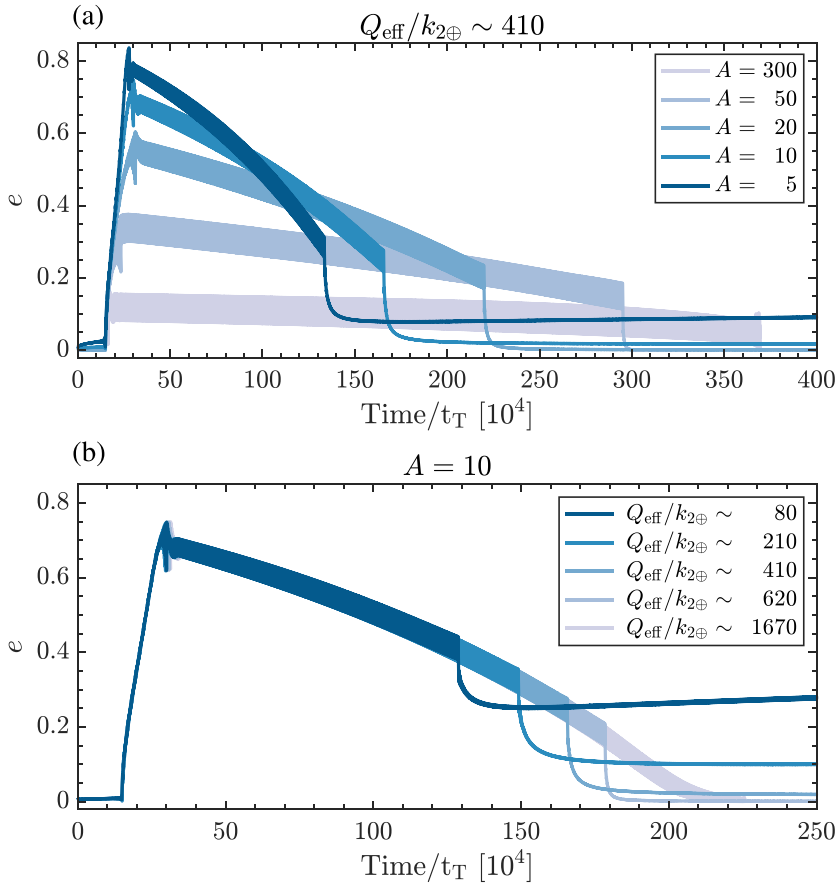

Figure 5. Eccentricity evolution with different (a) relative tidal strength values, A (assuming terrestrial tidal parameters $Q_{\rm eff}/k_{2\oplus} \sim 410$); (b) terrestrial tidal parameters, $Q_{\rm eff}/k_{2\oplus}$ (assuming $A = 10$). The time is normalized by the tidal timescale rate, t_T (see text) and assumes a nonsynchronous lunar rotation. For larger values of A with fixed $Q_{\rm eff}/k_{2\oplus}$, the maximum eccentricity excited during evection resonance decreases. When QR escape occurs, the evolution of the Moon's eccentricity shifts from an oscillating behavior whose value is controlled by evection to a standard evolution controlled by tides. For larger values of $Q_{\rm eff}/k_{2\oplus}$ with fixed A, the exit from the QR regime occurs later and at smaller eccentricities. With $A = 10$ and $Q_{\rm eff}/k_{2\oplus} \gtrsim 1,670$, the cosynchronous state in which the lunar month equals the Earth's day is achieved.

than $e_{\rm crit}$, preventing capture into evection resonance (e.g., for $Q_{\rm eff}/k_{2\oplus} = 42$ capture requires $A \lesssim 40$; see Figure S5a). Furthermore, for fast terrestrial tidal rates (small values of t_T or equivalently small $Q_{\rm eff}/k_{2\oplus}$) the minimum required eccentricity, $e_{\rm crit}$, increases, precluding capture into evection (e.g., for $A = 50$ capture occurs when $Q_{\rm eff}/k_{2\oplus} \gtrsim 210$; see Figure S5b). Overall, for large values of A and fast terrestrial tidal rates, the Moon exits proper evection before the resonance is fully developed, and Earth-Moon AM remains high.

For cases that result in initial capture into evection resonance, Figure 5shows the evolution of the eccentricity given different relative strength values, A, and different absolute tidal rates (represented by $Q_{\rm eff}/k_{2\oplus}$). For cases with $A < 4$, the eccentricity excitation is large, and the Moon's perigee becomes smaller than a high-e tidal disruption boundary, $q' < 2\ R_\oplus$ (Sridhar & Tremaine, 1992); therefore we considered $A \geq 5$. For increasing tidal dissipation inside the Moon (higher A), the maximum eccentricity reached is smaller (Figure 5a), because stronger lunar tides overcome Earth tides at a smaller eccentricity.

The angular momentum at the end of proper evection is $L'_{\rm esc} \approx a'^{7/4}_{\rm esc}(1-e^2_{\rm esc})/\Lambda + \gamma\sqrt{a'_{\rm esc}(1-e^2_{\rm esc})}$, where we assumed that the lunar spin contribution is small and that during resonance $\dot{\varphi} \approx 0$; hence $s' \approx a'^{7/4}(1-e^2)/\Lambda$. For lower A values, $a'_{\rm esc}(1-e^2_{\rm esc})$ decreases (see Figure S6), so that $L'_{\rm esc}$ is smaller; therefore more AM is removed during evection proper. However for low A and high-e evolutions, the assumption here that the lunar time delay is constant with time is not a good approximation. Tian et al. (2017) showed that tidal

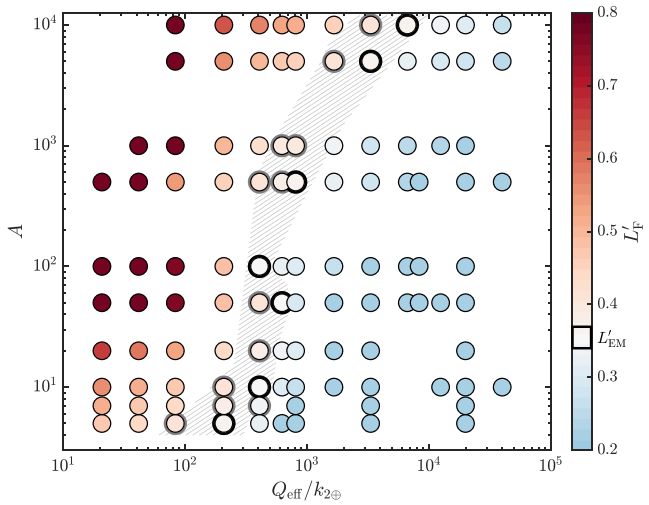

Figure 6. The final AM as a function of the initial terrestrial tidal parameters, $Q_{\rm eff}/k_{2\oplus}$, and the relative tidal strength factor, A, for the cases in which the Moon's rotation evolves solely due to tides (i.e., nonsynchronous lunar spin for eccentric orbits) and the tidal parameters are assumed to be constant with time. The initial AM for these simulations is $L' \sim 0.77$ (2.2 $L_{\rm EM}$), and the cosynchronous state has $L' \sim 0.23$ (~0.6 $L_{\rm EM}$), which is the minimum final AM. For each combination of A and $Q_{\rm eff}/k_{2\oplus}$, 10 initial $\varphi(0)$ values were simulated. The dispersion of the final AM in each combination is mostly dependent on whether the system exits the evection proper regime on the QR side or not. In the figure we show the minimum final AM in each combination, obtained in the simulations that exited on the QR side. We define the range of successful simulations with 0.99–1.07 $L_{\rm EM}$ (black circles), and in addition we highlight cases whose final AM lie outside the successful range but within the range 0.97–1.21 $L_{\rm EM}$ (gray circles). The former accounts for AM alterations due to late accretion (Bottke et al., 2010) and solar tides (Canup, 2004). The later range was arbitrarily chosen to reflect approximately 3 times more AM alteration than expected from these subsequent processes.

heating in the Moon during such high-e evolutions would lead to melting and increased lunar dissipation, ultimately causing early exit from evection (we return to this point in section 4).

For $A \gtrsim 400$, the overall excitation of eccentricity and semimajor axis during evection resonance is minimal, and there are no real solutions for Equation 13; hence while the stable stationary eccentricity, e_s, is small, the saddle stationary point is $e_{sx} = 0$ (this regime is referred to as the shallow resonance; Figures 2a and 2b). In this case, the central circulating region of clockwise motion (Figures 2c and 2d) does not exist, and escape from proper evection always occurs on the QR side.

To explain the differences in the timing of QR escape (Figure 5b), we combine the circulation timescale (Equation 14) and the crossing timescale (Equation 15) and define the minimum distance from the separatrix needed to maintain the system in QR:

$$e - e_{sx} = \frac{\pi |\dot{e}_{\oplus} + \dot{e}_m|}{2 t_T \Omega_{\odot} \sqrt{5\alpha} e_*} \tag{16}$$

Hence, with slower terrestrial tidal rates (larger t_T or $Q_{\rm eff}/k_{2\oplus}$) the eccentricity more closely approaches the separatrix before exiting the QR regime, resulting in more AM removal. For slow enough terrestrial tidal rates, QR drives the system all the way to the dual synchronous state (light blue curve in Figure 5b; see also Figure S7), assuming that the tidal parameters Δt and A remain unchanged during the evolution.

Moreover, because the eccentricity excitation is shallower as A increases (Figure 5a), the tidal derivative magnitude, $|\dot{e}_{\oplus} + \dot{e}_m|$, is lower as well. Therefore, with larger A values, the exit from QR regime occurs at a lower eccentricity as well, although the dependence is less substantial.

In general, the two tidal parameters, A and $Q_{\rm eff}/k_{2\oplus}$, have opposing effects on the final AM. As A increases for fixed $Q_{\rm eff}/k_{2\oplus}$, the final AM increases (less AM is removed), because the eccentricity excitation is lower. However, as $Q_{\rm eff}/k_{2\oplus}$ increases for fixed A, the final AM decreases (more AM is removed) because the system stays in QR longer and exits QR at a lower eccentricity. Hence, parameters that could produce a final AM of ~1 $L_{\rm EM}$ are correlated and follow the narrow inclined shaded band in Figure 6.

Although the A and $Q_{\rm eff}/k_{2\oplus}$ values appropriate during the Moon's encounter with evection are uncertain, a compelling argument has been made by Zahnle et al. (2015) that both would have been large. The Moon-forming impact would have likely heated Earth's mantle to an initially molten, fluid-like state (Nakajima & Stevenson, 2015), implying $Q \sim 10^3$ to 10^5, based on analogy to gas giant planets (e.g., Lainey et al., 2009, 2012, infer $Q/k_2 \approx 9 \times 10^4$ for Jupiter and $\approx 4 \times 10^3$ for Saturn, respectively). As Earth's mantle later began to solidify, its viscosity would have increased by orders-of-magnitude, causing greatly increased tidal dissipation and low Q values of order unity. However, there is a limit to how soon the Earth's mantle could have transitioned to this low-Q state, due to the volatile-rich atmosphere that would have persisted for a few Myr and controlled the rate of planet cooling. Consider a mantle that has started to solidify. If tidal heating exceeds what can be accommodated via atmospheric cooling, mantle temperatures would increase and the mantle crystal fraction would decrease, causing the mantle viscosity to decrease and with it tidal dissipation/heating. Conversely, if tidal dissipation in the mantle generated less heat than accommodated via radiative cooling, additional mantle freezing would occur, causing the mantle viscosity and tidal dissipation/heating to increase. Zahnle et al. (2015) argue that this feedback would cause Earth's initial tidal dissipation rate to be regulated by the modest cooling rate of its early dense atmosphere, yielding large initial terrestrial Q values that are similar to those inferred for giant planets when the Moon encountered evection.

Such slow orbital expansion rates would promote initial capture into evection resonance and imply that the Moon reaches the evection resonance point, a'_{res}, in approximately few $\times 10^5$ to few $\times 10^6$ year. Compared to this timescale, the lunar crustal formation time is fast ($\sim 10^3$ year for solidification of 80% of the magma ocean and lid formation Elkins-Tanton et al., 2011). In a partially solid early Moon, tidal dissipation is expected to be relatively high (i.e., large Δt_m), comparable to or higher than in the current Moon. Therefore the relative tidal strength, A, during evection would be high as well. Assuming lunar dissipation similar to the current value, Zahnle et al. (2015) estimated $A_Q \sim 10^2 - 10^4$ when the Moon encounters evection (note that their results are described by the parameter A_Q which is consistent with the constant-Q model and is a factor of $n/(s-n) \sim \mathcal{O}(10^{-1})$ smaller than the A used here from Equation 9). The likely presence of a lunar magma ocean when evection resonance occurs would increase tidal dissipation in the early Moon compared to that in the current Moon, hence increasing A even further.

Assuming that the terrestrial and lunar tidal parameters are constant throughout the evolution (i.e., that Δt and A are constant; see section 3.4 for cases in which these tidal parameters vary with time as Earth cools), the cosynchronous state is the most common final state across the range $10^3 < Q_{\rm eff}/k_{2\oplus} < 10^5$ and $10^2 < A < 10^4$ (blue markers in Figure 6). A small part of this range, for example, for $A \sim 10^4$ and $Q_{\rm eff}/k_{2\oplus} \sim 4 \cdot 10^3$, is consistent with the final AM of 1 $L_{\rm EM}$ (markers highlighted by the black circles in Figure 6).

3.3. Synchronous Lunar Spin

The above simulations assume that the lunar spin evolves solely due lunar tidal torques (Equation 4). These produce an approximately synchronous rotation for nearly circular orbits but yield $s_m > n$ for eccentric orbits. However, a tri-axial lunar shape (frozen in during lunar cooling; e.g., Garrick-Bethell et al., 2006) can maintain a synchronous spin even when the orbit is substantially eccentric if the figure torque is larger than the tidal torque (Goldreich & Peale, 1966). In this case, $s'_m = n'$ (where $n' \equiv a'^{-3/2}$ is the normalized lunar mean motion), and the Moon's spin is altered by both lunar tides and the permanent figure torque. We note that although the lunar lag angle when the Moon is in synchronous rotation is zero ($\delta_m = (s_m - n)\Delta t_m = 0$), dissipation of energy still occurs with Mignard tides for nonzero eccentricity, due to variations in the magnitude of the tide from periapse to apopase (Burns, 1986). Thus, even with $s_m = n$, there are changes in the Moon's orbit due to lunar tides if its orbit is noncircular (see also Text S1).

For a Moon with principal moments of inertia $C_m \geq B_m \geq A_m$, the orbit-averaged value of the permanent figure torque (pf) is (e.g., Goldreich & Peale, 1966):

$$\langle T_{pf} \rangle = -\frac{3}{2}\Omega_\oplus^2 \, a'^{-3/2}(B_m - A_m)\mathscr{K}(e)\sin 2\psi_0 = (\Omega_\oplus / t_T) C_m \dot{s}'_{m,\,pf} \tag{17}$$

where $\mathscr{K}(e) = 1 - 5e^2/2 + 13e^4/16$ is the so-called Hansen polynomial, ψ_0 is the angle between the long axis of the Moon and the Earth-Moon line at perigee, and $\dot{s}'_{m,\,pf}$ is the normalized resulting change in the lunar spin rate. This torque leads to additional contributions to $\dot{a}'$ and $\dot{e}$, which we parameterize as (Ward et al., 2020)

$$\frac{\dot{a}'_{pf}}{a'} = -f_{pf}\left[\frac{\dot{a}'_m}{a'} - \frac{2e\dot{e}_m}{1-e^2}\right] \tag{18}$$

$$\dot{e}_{pf} = \frac{g_{pf}}{2e}\left[\frac{\dot{a}'_m}{a'} - \frac{2e\dot{e}_m}{1-e^2}\right] \tag{19}$$

where $f_{pf} = \sqrt{1-e^2}$ and $g_{pf} = (1-e^2)(1-\sqrt{1-e^2})$; to second order in e, Equations 18 and 19 expressions are comparable to those used in prior studies (see Text S1).

Synchronous rotation can be maintained if $\dot{s}'_{m,\,pf}$ approximately balances that due to lunar tides, $\dot{s}'_m$, with the angle ψ_0 adopting the needed value. However $|\sin 2\psi_0|$ has a maximum value of unity, so that there is a minimum value of $(B_m - A_m)/C_m$ needed for $\dot{s}'_{m,\,pf} \approx |\dot{s}'_m|$

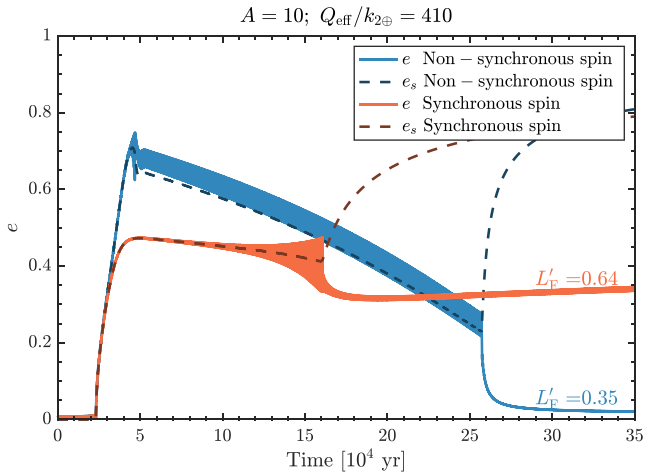

Figure 7. Evolution of the eccentricity (solid lines) and stable stationary eccentricity (dashed lines) for nonsynchronous (blue) and synchronous lunar rotation cases (orange). The latter includes the effect of permanent figure torques that are assumed to maintain the synchronous rotation (see text for details). The synchronous case experiences a smaller eccentricity excitation, and its libration amplitude growth while in resonance is more gradual, allowing the Moon to remain in evection proper for longer (until $t \sim 16 \times 10^4$ year) compared to the nonsynchronous case (that exits proper resonance at $t \sim 4.5 \times 10^4$ year). For all simulated cases with $A \leq 100$, the exit from evection proper for the synchronous case occurs below the stable eccentricity as is the case here, so that there is no QR regime. However, as discussed in the text it is not clear that synchronous rotation could be maintained for these low-A cases that lead to substantial lunar eccentricities. The final normalized AM is listed above each case.

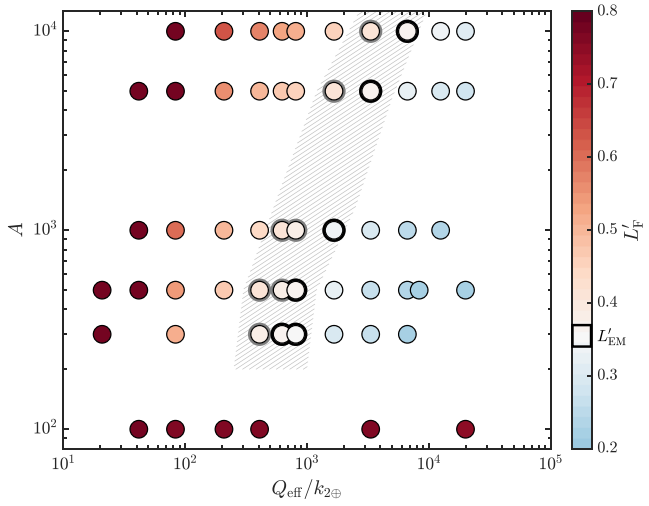

Figure 8. Similar caption to Figure 6 for cases that include the permanent figure torque (synchronous lunar spin). For tested simulations with $A \leq 100$, the Moon did not enter the QR regime, hence the AM remains high.

$$\frac{B_m - A_m}{C_m} > \left| \frac{\gamma}{3\kappa} \left(\frac{a'^{7/2}}{\Omega_\oplus t_T} \right) \frac{\sqrt{1-e^2}}{\mathscr{H}(e)} \left(\frac{\dot{a_m'}}{a'} - \frac{2e\dot{e}}{1-e^2} \right) \right|$$
$$> \left| 4 \times 10^{-4} \left(\frac{k_m \Delta t_m}{4\text{min}} \right) \left(\frac{7}{a'} \right)^{9/2} \frac{\sqrt{1-e^2}}{\mathscr{H}(e)} \left[f_1 - f_2 - \frac{e^2}{1-e^2}(g_1 - g_2) \right] \right| \quad (20)$$

where $k_m \Delta t_m \approx 4$ min for the current Moon (Williams & Boggs, 2015). If this condition is not met, nonsynchronous motion will result. For a low-eccentricity orbit, a value comparable to that for the current Moon's shape, $(B_m - A_m)/C_m = 2.28 \times 10^{-4}$ (Yoder, 1995), could maintain synchronous lock at the time of evection encounter. However, as e increases, a progressively larger value is needed; for example, for $e = 0.5$, $(B_m - A_m)/C_m > 10^{-2}$ is required, which may be difficult to maintain. Thus, a synchronous rotation model would seem most aptly applied to high A cases (in which the lunar eccentricity remains modest), while nonsynchronous rotation may be more likely for low A cases in which e achieves large values.

Figure 7 shows the eccentricity evolution for a synchronous case (orange line) compared to a nonsynchronous case (blue line). The maximum eccentricity before the orbital contraction is lower in the synchronous case, and the libration amplitude growth is more gradual; therefore the system remains in evection proper longer compared to the nonsynchronous case (as predicted by Ward et al., 2020).

For the cases we have tested with synchronous rotation and $A \leq 100$, exit from evection proper always occurs toward the central non-resonant region (or below the stable eccentricity; dashed line in Figure 7), and no quasi-resonant evolution occurs. The permanent figure torque causes an enhanced damping of the Moon's eccentricity compared to that due to lunar tides alone (i.e., Equation 19 is always negative), with the magnitude of the $\dot{e}_{pf}$ term depending on both A and the f and g functions, which in turn depend on e. Because the eccentricity as the Moon exists evection resonance increases as A decreases, the $\dot{e}_{pf}$ term actually becomes stronger as A decreases. For low enough A, when resonant control of e ends, the $\dot{e}_{pf}$ term is strong enough to pull the trajectory directly downward on the level curve diagram into the central region, precluding establishment of the QR for synchronous rotation cases with $A \leq 100$ (with little change in the AM; dark red markers in Figure 8 each representing 10 simulations with different initial φ). However, per above, (i) it is not clear that low-A/high-e cases would be consistent with synchronous rotation, and (ii) low-A/high-e cases would likely rapidly transition to high-A, due to the effects of tidal heating within the Moon for high e (Tian et al., 2017).

For cases with $A \gtrsim 300$, the eccentricity excitation is small, and the region below the separatrix does not exist ($e_{sx} = 0$). Hence, similar to the nonsynchronous cases, exit from evection proper always occurs toward the QR region. For low eccentricities associated with high-A cases, the additional permanent figure terms are small ($f_{pf} \approx 1$ and $g_{pf} \approx 0$); therefore, the timing of QR escape (governed by Equation 16) and the final Earth-Moon AM (Figure 8) is similar to the nonsynchronous case.

3.4. Effects of Planetary Cooling: $Q(t)$

The simulations above consider constant tidal parameters (Δt and A) throughout the evolution. Earth's early opaque atmosphere would have

kept its mantle molten and its Q very large for 2 to 5 Myr after a high-AM giant impact (Zahnle et al., 2015). After this time the mantle viscosity increases dramatically over the next few Myr as the mantle begins to freeze, which causes Q to plummet to values ~ unity (Zahnle et al., 2015). The time needed for the Earth's mantle to begin to solidify is typically somewhat shorter than the total time required for passage through evection proper and QR (e.g., for $Q_{\rm eff}/k_{2\oplus} \sim 10^4$ and $A = 5{,}000$, QR escape occurs at ~20 Myr). Therefore, while large Q likely applied when the Moon was captured into evection resonance, during the QR regime it may have decreased dramatically.

To estimate the effect of planetary cooling, we performed additional simulations with a varying terrestrial time lag, Δt. We assume that Earth's tidal dissipation factor, Q, evolves according to Zahnle et al. (2015), Figure 8, which depicts Earth's thermal evolution after a high-AM impact. We consider either a peak value of $(Q/k_{2\oplus}) \approx 7 \times 10^3$ (solid curves in Zahnle et al., 2015, their Figure 8) or $(Q/k_{2\oplus}) \approx 7 \times 10^4$ (dashed curves in Zahnle et al., 2015, their Figure 8).

For each time step, i, we calculate Earth's time lag according to

$$\Delta t_i = \frac{1}{2\Omega_{\oplus}(s'_{i-1} - n'_{i-1})Q_{\rm Zahnle,\,i}} \tag{21}$$

where s' and n' are sampled from previous time step, $i-1$, and $Q_{{\rm Zahnle},i}$ evolves with time per the Zahnle et al. model. The relative strength of lunar tides compared with Earth tides is calculated using

$$A_i = A_{\rm today}\left(\frac{\Delta t_{\rm today}}{\Delta t_i}\right)\left(\frac{k_{2,\,\oplus}}{k_{2,\,\rm fluid}}\right)\left(\frac{\Delta t_m}{\Delta t_{m,\,\rm today}}\right) \tag{22}$$

where $\Delta t_{\rm today}$ [$\Delta t_{m,{\rm today}}$] is Earth's [lunar] current time lag, we set $k_{2,{\rm fluid}} = 1.5$ as in Zahnle et al. (2015), and $A_{\rm today} \sim 13$ is the current ratio (assuming values of $k_{2m} = 0.024$, $\Delta t_{m,{\rm today}} = 165$ min, Williams & Boggs, 2015; $k_{2\oplus} = 0.30$ and $\Delta t_{\rm today} = 10$ min, Murray & Dermott, 1999). For a large terrestrial Q, the Moon evolves outward slowly and has time to partially solidify by the time evection resonance is encountered, leading to strong dissipation in the Moon comparable to or greater than in the Moon today (Zahnle et al., 2015). During initial evection resonance capture, A will be high; therefore the eccentricity excitation is low, and minimal heating inside the Moon due to evection is expected (Tian et al., 2017). Accordingly, we assume that the lunar lag time is constant throughout the evolution. The current lunar time delay is due to monthly dissipation as the Moon is synchronously rotating, but the Moon's rotation state and time delay during evection resonance and QR are uncertain. To account for the uncertainty on the appropriate lunar time lag during the evolution (e.g., the last 20% of the magma ocean solidification requires 10 Myr due to formation of anorthositic crust Elkins-Tanton et al., 2011), we consider different values for $f_m \equiv \Delta t_m/\Delta t_{m,{\rm today}}$. Values of $f_m > 1$ imply more tidal dissipation in the early Moon than in the Moon today, representing possible enhanced dissipation due to an early lunar magma ocean.

Figure 9 shows the lunar eccentricity evolution with peak $(Q_{\rm Zahnle}/k_{2,{\rm fluid}})$ values comparable to those inferred for Jupiter and Saturn from astrometry (Lainey et al., 2009, 2012) and assuming nonsynchronous lunar rotation. The Moon is captured into evection proper at 2.1 Myr [0.2 Myr] for the higher [lower] initial dissipation factor, followed by escape and a QR regime. As the tidal parameter, A, begins to rapidly decrease due to Earth's mantle cooling (lighter colors in Figures 9b and 9c), the eccentricity increases during the QR regime as lunar tides become less efficient compared to the strengthening Earth tides. For the slower tidal evolution (higher initial dissipation factor; blue curve in Figure 9d), most of the AM removal occurs after the mantle begins to solidify and $(Q_{\rm Zahnle}/k_{2,{\rm fluid}})$ drops (~6.5 Myr). QR escape occurs at ~6.9 Myr when the timescale of circulation is comparable to the timescale of tidal changes (Figure S8). In contrast to the constant time lag case (section 3.2), during Earth's cooling, the stable eccentricity gradually grows (level curves evolve outward from shallow resonance, Figure 2a, to deep resonance, Figure 2d). Eventually Earth's tidal strength increases (due to the sharp decrease in Earth's tidal dissipation factor; Figure 9a) at a rate that is comparable to the period of lunar circulation in QR ($t_{\rm cross} \sim P_{\rm circ}$; see Figure S8), and exit from QR occurs. In both $(Q_{\rm Zahnle}/k_{2,{\rm fluid}})$ evolutions the final system is left with too much AM for consistency with the Earth-Moon (Figure 9d). The mismatch worsens if, as is expected, early lunar dissipation was higher than in the current Moon ($f_m > 1$; dashed lines in Figure 9d).

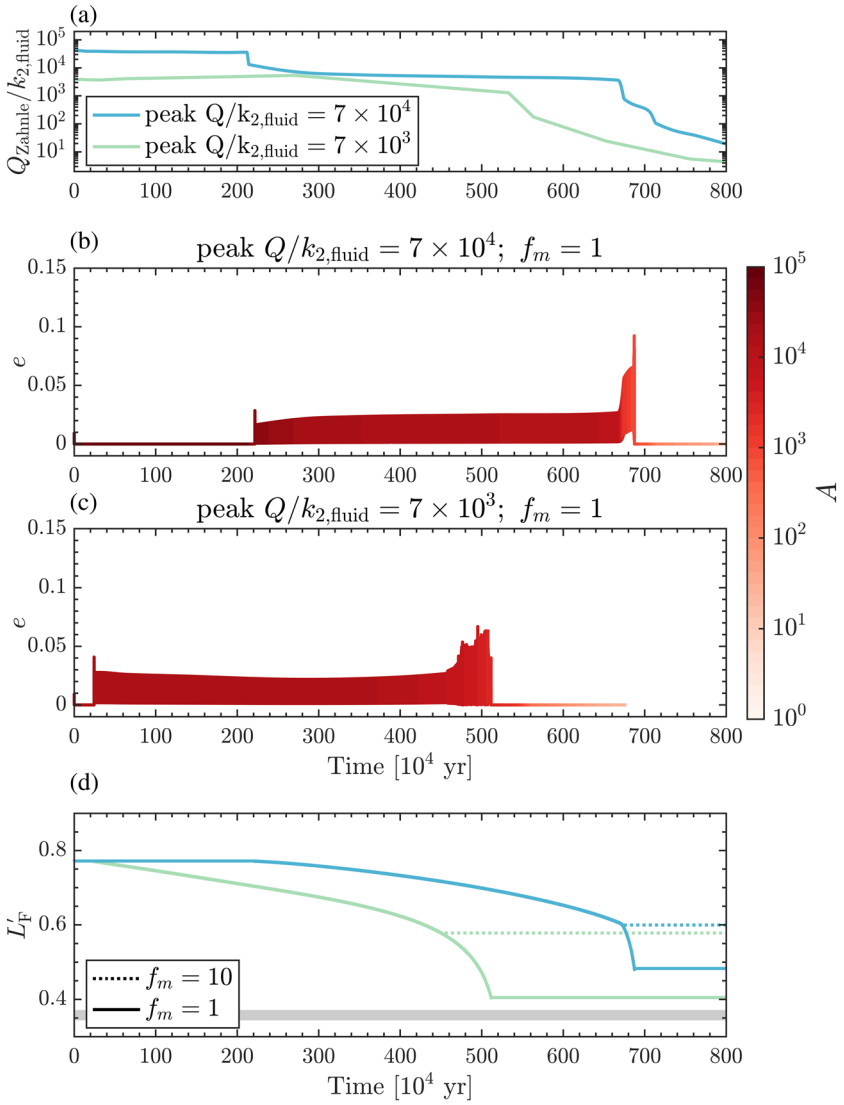

Figure 9. Evolution through evection resonance and the subsequent QR-regime with time-dependent tidal dissipation in the Earth and a nonsynchronous lunar rotation. (a) Time-dependent terrestrial tidal dissipation factor model by Zahnle et al. (2015) after a high-AM Moon forming impact (the low and middle curves in their Figure 8). The higher (blue) and lower (green) peak terrestrial ($Q/k_{2,\rm fluid}$) values are comparable to values inferred from astrometry for Jupiter and Saturn (Lainey et al., 2009, 2012). Lunar eccentricity during passage through evection assuming (a) a peak $Q/k_{2,\rm fluid} = 7 \times 10^4$ and $f_m = 1$; (b) a peak $Q/k_{2,\rm fluid} = 7 \times 10^3$ and $f_m = 1$. The evolution of the relative tidal strength, A, is indicated by the red colors. (d) Normalized AM evolution of the Earth-Moon system for $f_m = 1$ (i.e., with lunar tidal parameters comparable to those in the current Moon; solid line) and $f_m = 10$ (corresponding to enhanced dissipation in the early Moon due to the presence of a magma ocean; dashed line), for the higher (blue) and lower (green) peak terrestrial $Q/k_{2,\rm fluid}$ cases. The horizontal gray area represents values consistent with the current Earth-Moon, accounting for later AM change due to solar tides and late accretion impacts (Bottke et al., 2010; Canup, 2004).

4. Conclusions and Discussion

In this work we modeled the lunar tidal evolution during its encounter with the evection resonance. The Moon tidally recedes away from its accretion location near the Roche limit, while its perigee precession period increases. The Moon encounters evection resonance when the precession period equals 1 year. During evection proper, the eccentricity increases, and the Moon librates around the stable stationary point, $\varphi \sim \pm\pi/2$ (representing the angle between the Moon's perigee and the Sun). As the eccentricity increases, lunar tides (governed by the tidal parameter A) become stronger and eventually cause the lunar orbit to contract.

During resonance, the solar net torque controls the Moon's eccentricity, while tides still control the evolution of the Moon's semimajor axis, and the balance between the lunar orbital angular momentum (AM) and the spins of the Earth and Moon (Equation 1) can no longer be maintained. As such, AM is removed from the Earth-Moon system and transferred to the Earth's heliocentric orbit. Near the turn-around point, when the Moon's orbit begins to contract, the libration amplitude increases and leads to escape from proper resonance. This is consistent with escape timing seen in Touma and Wisdom (1998) with the Mignard model for initial AM values of $\sim L_{\rm EM}$ and with analytic predictions of libration growth in Ward et al. (2020).

If the lunar spin evolves only due to tides, once the orbit contracts and exits evection proper, it typically enters a quasi-resonance (QR) regime. Although the Moon is not librating around a stationary point and thus is not in formal resonance, evection still regulates the eccentricity evolution during QR, and it is during the QR-regime that substantial AM can be removed from the Earth-Moon pair. The QR regime is reminiscent of the limit cycle found by Wisdom and Tian (2015) and thus is probably not an artifact of the chosen tidal model (Mignard vs. constant-Q tides). We find that for Mignard tides, the final AM depends on the timing of QR escape, and prolonged occupation of the QR state may result in a cosynchronous state, inconsistent with the Moon's long-term survival.

If the Moon had a permanent frozen figure that maintains synchronous rotation even when its orbit is eccentric, additional terms to the eccentricity and semimajor axis evolution apply. In this case, for relatively weak lunar tides ($A < 300$), the Moon always exits the proper evection regime on the non-QR side of the resonance; hence overall only minimal AM is removed. In addition, for very low A, tidal heating in the Moon would likely lead to rapid escape from resonance (Tian et al., 2017, see below). For stronger lunar tides ($A > 300$), the eccentricity excitation is small and the additional permanent figure terms are negligible, yielding similar results as the nonsynchronous case.

For constant tidal parameters, our results imply that only for a narrow range in both A and $Q_{\rm eff}/k_{2\oplus}$ would a post-giant impact system with about twice the AM of the Earth-Moon system have its AM appropriately reduced to $\sim L_{\rm EM}$ by the evection resonance. Our results do not show a preference for creating final systems with an AM comparable to that of the Earth-Moon. This contrasts with the findings of Ćuk and Stewart (2012), who argued that for a certain range of A, final systems with $L_{\rm F} \sim L_{\rm EM}$ would always result so long as Q was large enough to allow initial capture into resonance. We instead find that the final system AM varies greatly even for a given A, for different $Q_{\rm eff}/k_{2\oplus}$ values.

The Earth's mantle likely remained molten and fluid-like in its tidal response for few $\sim 10^6$ years due to the Earth's thermally blanketing atmosphere, while the Moon would have more rapidly cooled to a partially solid, tidally dissipative state (Zahnle et al., 2015). Thus the physically most plausible conditions when the Moon encountered evection resonance are low Δt (high $Q_{\rm eff}$) and high A (Zahnle et al., 2015). For this combination, and assuming fixed (i.e., non-time dependent) values for Δt and A, we find that evection resonance and the subsequent QR-regime typically removes too much AM and often leaves the system in the dual synchronous state in which the lunar month equals the terrestrial day. The latter would ultimately lead to the loss of the Moon as the Earth's spin was further slowed by solar tides, causing the Moon to then lie inside corotation and be subject to inward tidal evolution.

However, tidal parameters may have instead changed with time during the Moon's interactions with evection resonance and the subsequent QR-regime. For low-A cases that lead to large evection-resonance-driven lunar eccentricities, Tian et al. (2017) showed that tidal heating in the Moon causes rapid escape from evection resonance as the lunar tidal Q-value decreases, resulting in insufficient AM removal.

For the high-A cases advocated here and in Zahnle et al. (2015), excitation of the lunar eccentricity by evection resonance is modest, and tidal heating in the Moon would be unlikely to substantially affect the lunar tidal parameters (Tian et al., 2017). For high-A cases, it is instead the time evolution of the Earth's Q value as its mantle began to freeze that is important to consider. We adopt the time-dependent Q model of Zahnle et al. (2015) and find that escape from QR occurs early, so that the final system is left with an AM substantially larger than in the Earth-Moon. Zahnle et al. (2015) point out that the predicted Q as a function of the Moon's semimajor axis (or alternatively, Q as a function of time) is essentially constant across many assumed atmospheric and albedo conditions, so long as the terrestrial mantle after the giant impact was sufficiently molten that it responded like a low viscosity liquid. Because the latter appears highly probable (Nakajima

& Stevenson, 2015), a successful outcome in which the final system AM is $\sim L_{\rm EM}$ after evection resonance and a subsequent QR-regime may be difficult to achieve. It is, however, possible that a constant lag angle model could yield different results than those seen here with Mignard tides, as the effect of a time-varying terrestrial Q was not considered in the limit cycle analysis of Tian et al. (2017).

Additional AM removal processes (e.g., solar tides Canup, 2004, late veneer impacts; Bottke et al., 2010, core/mantle friction Goldreich & Peale, 1970) appear to have a small effect on the final AM of the system. Alternatively, if Earth's obliquity was >65° after the Moon-forming impact, the Moon could encounter an instability during the Laplace plane transition (occurring when the effects of Earth's oblateness on the lunar precessional motion are comparable to those of the Sun). During the instability, Earth's spin decreases and AM is transferred to Earth's orbit (Ćuk et al., 2016). However, Tian and Wisdom (2020) argue that such an evolution cannot reproduce the current Earth-Moon system, because the needed initial high-obliquity state is inconsistent with the component of the current Earth-Moon angular momentum that is perpendicular to the ecliptic plane.

Data Availability Statement

The equations provided in the main text and in the referenced works provide all information needed to reproduce the results presented in the manuscript. The numerical results presented in Figures 6 and 8 are provided in Tables S2 and S3, respectively, available for download at: https://doi.org/10.5281/zenodo.3981508.

Acknowledgments

This paper is dedicated to the memory of William R. Ward. This research was supported by NASA's SSERVI and Emerging Worlds programs. R. R. is an Awardee of the Weizmann Institute of Science - National Postdoctoral Award Program for Advancing Women in Science. We thank the anonymous reviewers for their comments that improved the final version of this manuscript.

References

Bottke, W. F., Walker, R. J., Day, J. M., Nesvorny, D., & Elkins-Tanton, L. (2010). Stochastic late accretion to E,arth, the Moon, and Mars. *Science*, *330*(6010), 1527–1530.

Brouwer, D., & Clemence, G. M (1961). *Methods of celestial mechanics*. New York: Academic Press.

Brown, P. N., Byrne, G. D., & Hindmarsh, A. C. (1989). VODE: A variable-coefficient ODE solver. *SIAM Journal on Scientific and Statistical Computing*, *10*(5), 1038–1051.

Burns, J. A. (1986). The evolution of satellite orbits, *Satellites* pp. 117–158). Tucson, AZ: University of Arizona Press.

Cameron, A. G., & Ward, W. R. (1976). The origin of the Moon. In *Lunar and Planetary Science Conference*, *7*.

Canup, R. M. (2004). Simulations of a late lunar-forming impact. *Icarus*, *168*(2), 433–456.

Canup, R. M. (2012). Forming a Moon with an Earth-like composition via a giant impact. *Science*, *338*(6110), 1052–1055.

Canup, R. M., & Asphaug, E. (2001). Origin of the Moon in a giant impact near the end of the Earth's formation. *Nature*, *412*(6848), 708.

Canup, R. M., Visscher, C., Salmon, J., & Fegley, Jr B. (2015). Lunar volatile depletion due to incomplete accretion within an impact-generated disk. *Nature Geoscience*, *8*(12), 918.

Ćuk, M., Hamilton, D. P., Lock, S. J., & Stewart, S. T. (2016). Tidal evolution of the Moon from a high-obliquity, high-angular-momentum Earth. *Nature*, *539*(7629), 402–406.

Ćuk, M., & Stewart, S. T. (2012). Making the Moon from a fast-spinning Earth: A giant impact followed by resonant despinning. *Science*, *338*(6110), 1047–1052.

Efroimsky, M., & Lainey, V. (2007). Physics of bodily tides in terrestrial planets and the appropriate scales of dynamical evolution. *Journal of Geophysical Research*, *112*, E12003. https://doi.org/10.1029/2007JE002908

Elkins-Tanton, L. T., Burgess, S., & Yin, Q.-Z. (2011). The lunar magma ocean: Reconciling the solidification process with lunar petrology and geochronology. *Earth and Planetary Science Letters*, *304*(3), 326–336.

Garrick-Bethell, I., Wisdom, J., & Zuber, M. T. (2006). Evidence for a past high-eccentricity lunar orbit. *Science*, *313*(5787), 652–655.

Goldreich, P. (1966). History of the lunar orbit. *Reviews of Geophysics*, *4*(4), 411–439.

Goldreich, P., & Peale, S. (1966). Spin-orbit coupling in the solar system. *The Astronomical Journal*, *71*, 425.

Goldreich, P., & Peale, S. (1970). The obliquity of Venus. *The Astronomical Journal*, *75*, 273.

Herwartz, D., Pack, A., Friedrichs, B., & Bischoff, A. (2014). Identification of the giant impactor Theia in lunar rocks. *Science*, *344*(6188), 1146–1150.

Ida, S., Canup, R. M., & Stewart, G. R. (1997). Lunar accretion from an impact-generated disk. *Nature*, *389*(6649), 353–357.

Kaula, W. M. (1964). Tidal dissipation by solid friction and the resulting orbital evolution. *Reviews of Geophysics*, *2*(4), 661–685.

Kaula, W., & Yoder, C. (1976). Lunar orbit evolution and tidal heating of the Moon. In *Lunar and Planetary Science Conference*, *7*.

Lainey, V., Arlot, J.-E., Karatekin, Ö., & Van Hoolst, T. (2009). Strong tidal dissipation in Io and Jupiter from astrometric observations. *Nature*, *459*(7249), 957–959.

Lainey, V., Karatekin, Ö., Desmars, J., Charnoz, S., Arlot, J.-E., Emelyanov, N., et al. (2012). Strong tidal dissipation in Saturn and constraints on Enceladus' thermal state from astrometry. *The Astrophysical Journal*, *752*(1), 14.

Lock, S. J., Stewart, S. T., Petaev, M. I., Leinhardt, Z., Mace, M. T., Jacobsen, S. B., & Cuk, M.(2018). The origin of the Moon within a terrestrial synestia. *Journal of Geophysical Research: Planets*, *123*, 910–951. https://doi.org/10.1002/2017JE005333

Meyer, J., Elkins-Tanton, L., & Wisdom, J. (2010). Coupled thermal-orbital evolution of the early Moon. *Icarus*, *208*(1), 1–10.

Mignard, F. (1979). The evolution of the lunar orbit revisited. I. *The Moon and the Planets*, *20*(3), 301–315.

Mignard, F. (1980). The evolution of the lunar orbit revisited, II. *The Moon and the Planets*, *23*(2), 185–201.

Murray, C. D., & Dermott, S. F. (1999). *Solar system dynamics*. Cambridge: Cambridge university press.

Nakajima, M., & Stevenson, D. J. (2015). Melting and mixing states of the Earth's mantle after the Moon-forming impact. *Earth and Planetary Science Letters*, *427*, 286–295.

Pahlevan, K., & Morbidelli, A. (2015). Collisionless encounters and the origin of the lunar inclination. *Nature*, *527*(7579), 492–494.

Peale, S., & Canup, R. (2015). The origin of the natural satellites, (2nd ed.). In G. Schubert (Ed.), *Treatise on Geophysics* (vol. 10, pp. 559–604). Oxford: Elsevier.
Salmon, J., & Canup, R. M. (2012). Lunar accretion from a Roche-interior fluid disk. *The Astrophysical Journal*, *760*(1), 83.
Salmon, J., & Canup, R. M. (2014). Accretion of the Moon from non-canonical discs. *Philosophical Transactions of the Royal Society of London A: Mathematical Physical and Engineering Sciences*, *372*(2024), 20130256.
Spurzem, R., Giersz, M., Heggie, D., & Lin, D. (2009). Dynamics of planetary systems in star clusters. *The Astrophysical Journal*, *697*(1), 458.
Sridhar, S., & Tremaine, S. (1992). Tidal disruption of viscous bodies. *Icarus*, *95*(1), 86–99.
Tian, Z., & Wisdom, J. (2020). Vertical angular momentum constraint on lunar formation and orbital history. *Proceedings of the National Academy of Sciences*, *117*(27), 15,460–15,464.
Tian, Z., Wisdom, J., & Elkins-Tanton, L. (2017). Coupled orbital-thermal evolution of the early Earth-Moon system with a fast-spinning Earth. *Icarus*, *281*, 90–102.
Touma, J., & Wisdom, J. (1994). Evolution of the Earth-Moon system. *The Astronomical Journal*, *108*, 1943–1961.
Touma, J., & Wisdom, J. (1998). Resonances in the early evolution of the Earth-Moon system. *The Astronomical Journal*, *115*(4), 1653.
Virtanen, P., Gommers, R., Oliphant, T. E., Haberland, M., Reddy, T., Cournapeau, D., et al. (2019). Scipy 1.0—Fundamental algorithms for scientific computing in python. arXiv preprint arXiv 190710121.
Ward, W. R., & Canup, R. M. (2013). The evection resonance and the angular momentum of the Earth-Moon system. In *Lunar and Planetary Science Conference*, *3029*.
Ward, W. R., Canup, R. M., & Rufu, R. (2020). Analytical model for the tidal evolution of the evection resonance and the timing of resonance escape. *Journal of Geophysical Research: Planets*, *125*, e2019JE006266. https://doi.org/10.1029/2019JE006266
Williams, J. G., & Boggs, D. H. (2015). Tides on the Moon: Theory and determination of dissipation. *Journal of Geophysical Research: Planets*, *120*, 689–724. https://doi.org/10.1002/2014JE004755
Williams, J. G., Konopliv, A. S., Boggs, D. H., Park, R. S., Yuan, D.-N., Lemoine, F. G., et al. (2014). Lunar interior properties from the GRAIL mission. *Journal of Geophysical Research: Planets*, *119*, 1546–1578. https://doi.org/10.1002/2013JE004559
Wisdom, J., & Tian, Z. (2015). Early evolution of the Earth-Moon system with a fast-spinning Earth. *Icarus*, *256*, 138–146.
Yoder, C. F. (1995). *Astrometric and geodetic properties of Earth and the solar system*, vol. 1. Washington, DC: Wiley Online Library.
Zahnle, K. J., Lupu, R., Dobrovolskis, A., & Sleep, N. H. (2015). The tethered Moon. *Earth and Planetary Science Letters*, *427*, 74–82.
Zhang, J., Dauphas, N., Davis, A. M., Leya, I., & Fedkin, A. (2012). The proto-Earth as a significant source of lunar material. *Nature Geoscience*, *5*(4), 251–255.